Geophys. J. Int. (1993) **114,** 433–442

Inversion of time-domain electromagnetic data for a horizontally layered Earth

C. G. Farquharson and D. W. Oldenburg

UBC-Geophysical Inversion Facility, Department of Geophysics & Astronomy, University of British Columbia, 129–2219 Main Mall, Vancouver, BC V6T 1Z4, Canada

Accepted 1992 December 15. Received 1992 November 25; in original form 1992 June 8

SUMMARY

Time-domain electromagnetic (TEM) data are inverted to produce a conductivity model composed of horizontal layers of constant conductivity. The data can be values of the time decay of the vertical component of the magnetic field, or of its time derivative, measured at points either inside or outside a rectangular transmitter loop. Our inversion allows many more layers than there are data. This means that the constructed conductivity model not only fits the data to the required level, but also possesses particular characteristics. By suitable choice of the objective function to be minimized, our constructed model may have minimum structure in some well-defined sense and/or it may be close to some known background model. Our inversion algorithm works directly in the time domain. This requires fractionally more computing time than the alternative approach of transforming the data to the frequency domain before inversion. However, working in the time domain prevents distortion of the data and their associated measurement errors which may arise during the transformation. Also, the effects of the full transmitter current waveform can easily be incorporated by convolution in the time domain. Our inversion is applied to data from an environmental survey and the results are shown to compare favourably with a nearby well-log.

Key words: electrical conductivity, electromagnetic surveys, inversion.

1 INTRODUCTION

Time-domain electromagnetic (TEM) soundings have a well-established place in exploration geophysics, and are in the vanguard of methods used in the ever expanding field of environmental geophysics. An excellent review of the TEM method and its uses is given by Nabighian & Macnae (1991). Typically, a step or ramp turn-off in the current flowing in a rectangular transmitter loop induces currents in the Earth, and the vertical component of the h field, or its time derivative, resulting from these induced currents is measured. These measurements can be at any point on the surface of the Earth, either inside or outside the transmitter loop.

TEM measurements are commonly interpreted using an imaging technique (e.g. Macnae & Lamontagne 1987; Nekut 1987; Eaton & Hohmann 1989; Fullager 1989) or a parametric inversion (e.g. Anderson 1982, 1985; Raiche *et al.* 1985; Huang & Palacky 1991). In the imaging methods, the downward and outward diffusion of the induced current system in the Earth is approximated by one or more image current loops that move downwards with time. The variation in the depth and speed of these image current loops with time can be converted into a conductivity–depth section that gives a smooth approximation to the true conductivity structure. These imaging techniques can be thought of as sophisticated transformations of the observed data. They are rapid to compute but the resultant conductivity is not, in general, consistent with the observations. In a parametric inversion, an over-determined least-squares problem is solved to find the thicknesses and conductivities of a limited number of layers, perhaps half-a-dozen, that most closely reproduce the observations. This approach has the potential for generating a plausible representation of the Earth. However, the results that are obtained depend on the assumed number of layers and on the starting model used in the iterative inversion.

In this paper, we present an alternative formulation. Our earth model is composed of horizontal layers of fixed thickness and constant conductivity, and is terminated by a half-space. Generally, we have many more layers than observations, so our inverse problem is under-determined.

This greatly increases the non-uniqueness of the mathematical solution but allows us to find, from the infinity of models that adequately reproduce the data, that one which minimizes a specific objective function of the model. Suitable choice of the objective function to be minimized will result in a model that is concordant with geological intuition and any prior geophysical knowledge. Ideally, the resulting model should exhibit the right 'character' (that is, smooth or blocky in accordance with the assumed geology), be as close as possible to the conductivity section obtained from a well-log or a neighbouring sounding (if such is available) and have a minimum amount of structure. This last point is particularly important since arbitrarily complicated structures, which would, therefore, seem unlikely to resemble the true Earth, can suffice as mathematical solutions. Our desire is to generate a model that contains just enough structure to fit the observations, but no more. The flexibility to generate models of a particular character enhances the usefulness of our inversion routine compared with those algorithms that concentrate only upon misfit as a criterion for an acceptable model.

An inversion formulation that admits a large number of layers is not entirely new for TEM data. Fullagar & Oldenburg (1984) treated the inversion of horizontal-loop frequency-domain data from this perspective, and Fullager (1983) applied the algorithm to data transformed from the time domain to the frequency domain. In his inversion, however, only the norm of the perturbation to the model is minimized at each iteration, rather than the norm of the model itself. Consequently, there is no ability to control the form of the model and so generate a final model having particular characteristics. Much of the advantage of using the under-determined formalism is lost. There is also the practical difficulty of transforming the observations to the frequency domain and, in particular, of ascribing meaningful errors to the transformed data.

The measurements obtained from a TEM experiment are values of the magnetic field, or its time derivative, as a function of time. Although our inversion works directly with these time-domain data, many of the basic computations are carried out in the frequency domain. In Section 2 we give a solution to the forward problem and show how to calculate the sensitivities needed to solve the inverse problem. Our method for solving the inverse problem is presented in Section 3, and in Section 4 it is applied to both synthetic and field data.

2 THEORY

2.1 The forward problem

We consider the forward problem of calculating either $h_z(t)$ or $\partial h_z(t)/\partial t$ induced at some point on the surface of a layered conductivity structure by a step turn-off in the current in a rectangular transmitter loop. Such a layered conductivity structure, along with the coordinate system used in this paper, is shown in Fig. 1.

To exploit the work that has been done on electromagnetic methods in the frequency domain, we shall carry out the analysis in the frequency domain and, only at the very end, transform the results to the time domain. Most of the derivation below is based upon the work of Kaufman & Keller (1983) and Ward & Hohmann (1988). We shall follow the notation of Ward & Hohmann and use lower case letters for fields in the time domain and upper case letters for fields in the frequency domain.

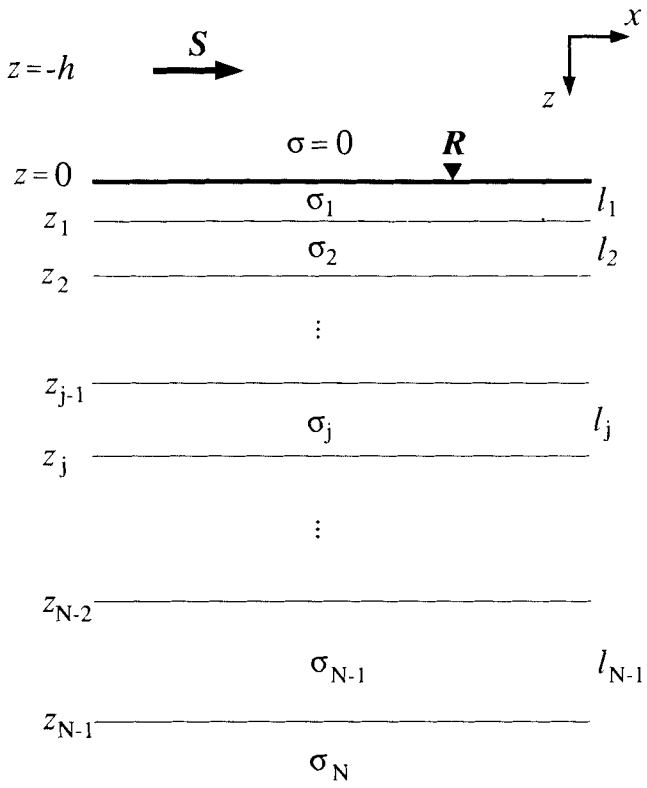

Figure 1. Notation and coordinate system for the horizontally layered conductivity model of the Earth used in this paper. z_j is the depth to the bottom of the jth layer, and σ_j and l_j are the conductivity and thickness, respectively, of the jth layer. S represents the source at a height h above the surface of the Earth, and R indicates the measurement location.

For the source-free region of Fig. 1, Maxwell's equations in the time domain are

$$\nabla \times \mathbf{e}(x, y, z, t) = -\frac{\partial}{\partial t}\mathbf{b}(x, y, z, t) \tag{1}$$

and

$$\nabla \times \mathbf{h}(x, y, z, t) = \mathbf{j}(x, y, z, t) + \frac{\partial}{\partial t}\mathbf{d}(x, y, z, t), \tag{2}$$

where $\mathbf{e}$, $\mathbf{b}$, $\mathbf{h}$ and $\mathbf{d}$ are the electric field intensity, the magnetic induction, the magnetic field intensity and the electric displacement, respectively. $\mathbf{j}$ is the electric current density. By assuming a time dependence of $e^{i\omega t}$, and making use of the constitutive relations for a linear, isotropic medium, namely $\mathbf{D} = \varepsilon_0\mathbf{E}$, $\mathbf{B} = \mu_0\mathbf{H}$ and $\mathbf{J} = \sigma\mathbf{E}$, the corresponding pair of equations in the frequency-domain is

$$\nabla \times \mathbf{E}(x, y, z, \omega) = -i\omega\mu_0\mathbf{H}(x, y, z, \omega) \tag{3}$$

and

$$\nabla \times \mathbf{H}(x, y, z, \omega) = (\sigma + i\omega\varepsilon_0)\mathbf{E}(x, y, z, \omega), \tag{4}$$

where σ is the electrical conductivity, and we have assumed for simplicity, that the magnetic permeability and the electric permittivity are everywhere equal to their free space values of μ_0 and ε_0 respectively. In fact, for the analysis in this paper, it is necessary only that the permeability and permittivity be constant and known in each layer.

The H field due to a rectangular transmitter loop can be evaluated by integrating the response of a horizontal electric dipole around the transmitter loop (Poddar 1982). Therefore, the major portion of the forward problem involves calculating $H_z(x, y, z, \omega)$ due to a horizontal dipole. To make use of the two axes of symmetry in this problem, one along the axis of the dipole and the other along the direction in which the conductivity is changing (i.e. the vertical direction in this 1-D earth), we introduce a vector potential $\mathbf{A}(x, y, z, \omega)$ such that

$$\mathbf{H}(x, y, z, \omega) = \nabla \times \mathbf{A}(x, y, z, \omega). \tag{5}$$

Substituting this expression for $\mathbf{H}$ into eq. (3) gives

$$\nabla \times \mathbf{E} = -i\omega\mu_0 \nabla \times \mathbf{A}, \tag{6}$$

which implies that, assuming a region of constant permeability, the electric field intensity can be written as

$$\mathbf{E} = -i\omega\mu_0 \mathbf{A} + \nabla U, \tag{7}$$

where U is some scalar potential. Substituting eq. (5) into eq. (4) gives

$$\nabla \times \nabla \times \mathbf{A} = (\sigma + i\omega\varepsilon_0)\mathbf{E}. \tag{8}$$

Using the vector identity $\nabla \times \nabla \times \mathbf{A} = \nabla\nabla \cdot \mathbf{A} - \nabla^2\mathbf{A}$, and the expression for the electric field intensity given in eq. (7), eq. (8) becomes

$$\nabla\nabla \cdot \mathbf{A} - \nabla^2\mathbf{A} = (\sigma + i\omega\varepsilon_0)(-i\omega\mu_0\mathbf{A} + \nabla U). \tag{9}$$

Since the scalar potential, U, is arbitrary, we can choose it such that $\nabla \cdot \mathbf{A} = (\sigma + i\omega\varepsilon_0)U$. Using this expression to eliminate U from eq. (9), assuming constant conductivity and permittivity, results in the differential equation for the vector potential:

$$(\nabla^2 + \mu_0\varepsilon_0\omega^2 - i\omega\mu_0\sigma)\mathbf{A}(x, y, z, \omega) = 0. \tag{10}$$

Because of the two symmetries mentioned above, the vector potential $\mathbf{A}$ need only have two components, one in the direction of the horizontal dipole and the other in the vertical direction. Taking the dipole to lie in the x direction, $\mathbf{A}$ has the form $\mathbf{A} = (A_x, 0, A_z)$. Moreover, because we are only interested in the vertical component of the H field, and because the relationship between $\mathbf{H}$ and $\mathbf{A}$ defined in eq. (5) now gives $H_z = -\partial A_x/\partial y$, we need only consider the x component of the vector potential $\mathbf{A}$ in future calculations.

Equation (10) is valid within each layer of Fig. 1. The continuity of the tangential components of $\mathbf{E}$ and $\mathbf{H}$ across each boundary leads to the following conditions for the x component of the vector potential:

$$\begin{aligned} A_x^j(x, y, z = z_j, \omega) &= A_x^{j+1}(x, y, z = z_j, \omega), \\ \frac{\partial}{\partial z} A_x^j(x, y, z = z_j, \omega) &= \frac{\partial}{\partial z} A_x^{j+1}(x, y, z = z_j, \omega), \end{aligned} \tag{11}$$

where the superscript denotes the layer.

To reduce the x component of eq. (10) to an ordinary differential equation in the variable z, we shall make use of the 2-D Fourier transform pair:

$$\begin{aligned} \tilde{F}(k_x, k_y, z) &= \int_{-\infty}^{\infty}\int_{-\infty}^{\infty} F(x, y, z) e^{-i(k_x x + k_y y)}\, dx\, dy, \\ F(x, y, z) &= \frac{1}{4\pi^2}\int_{-\infty}^{\infty}\int_{-\infty}^{\infty} \tilde{F}(k_x, k_y, z) e^{i(k_x x + k_y y)}\, dk_x\, dk_y. \end{aligned} \tag{12}$$

Applying this Fourier transform to the x-component of eq. (10) gives, for the jth layer,

$$\left(\frac{d^2}{dz^2} - u_j^2\right)\tilde{A}_x^j(k_x, k_y, z, \omega) = 0, \tag{13}$$

where $u_j^2 = k_x^2 + k_y^2 - \mu_0\varepsilon_0\omega^2 + i\omega\mu_0\sigma_j$. The solution of eq. (13) is

$$\begin{aligned} \tilde{A}_x^j(k_x, k_y, z, \omega) = {} & C_j(k_x, k_y, \omega) e^{[u_j(z - z_{j-1})]} \\ & + D_j(k_x, k_y, \omega) e^{[-u_j(z - z_{j-1})]}, \end{aligned} \tag{14}$$

where C_j and D_j are determined by the boundary conditions for $\tilde{A}_x$. These boundary conditions are obtained by applying the 2-D Fourier transform to eq. (11), giving

$$\begin{aligned} \tilde{A}_x^j(k_x, k_y, z = z_j, \omega) &= \tilde{A}_x^{j+1}(k_x, k_y, z = z_j, \omega), \\ \frac{\partial}{\partial z}\tilde{A}_x^j(k_x, k_y, z = z_j, \omega) &= \frac{\partial}{\partial z}\tilde{A}_x^{j+1}(k_x, k_y, z = z_j, \omega). \end{aligned} \tag{15}$$

In the basement half-space (layer N) the requirement that the magnetic field should decay to zero as z becomes large means that $C_N = 0$. At the top of the stack of layers, $\tilde{A}_x^1(k_x, k_y, z = 0, \omega)$ must match the solution in layer 0 of the inhomogeneous version of eq. (13) which results from the presence of the horizontal electric dipole. Kaufman & Keller (eq. 2.51) give the appropriate expression for $A_x(x, y, z, \omega)$ in the non-conducting half-space above a layered earth:

$$\begin{aligned} A_x^0(x, y, z, \omega) = {} & \frac{I\, ds}{4\pi}\int_0^{\infty}\left[\frac{\lambda}{u_0}\exp(-u_0|z + h|) + \hat{C}_0(\lambda, \omega)\exp(u_0 z)\right] \\ & \times J_0(\lambda r)\, d\lambda, \end{aligned} \tag{16}$$

where I is the current in the electric dipole, ds is the length of the dipole, $u_0^2 = \lambda^2 - \mu_0\varepsilon_0\omega^2$, $\lambda^2 = k_x^2 + k_y^2$, $r^2 = x^2 + y^2$, h is the height of the dipole above the surface of the Earth, J_0 is the zeroth order Bessel function and $\hat{C}_0$ is determined by the boundary conditions at $z = 0$. A Hankel transform can be converted to a 2-D Fourier transform using the relationship (Ward & Hohmann, eq. 2.10)

$$\begin{aligned} 2\pi\int_0^{\infty}\tilde{F}(\lambda)\lambda J_0(\lambda r)\, d\lambda &= \int_{-\infty}^{\infty}\int_{-\infty}^{\infty}\tilde{F}(k_k^2 + k_y^2) e^{i(k_x x + k_y y)}\, dk_x\, dk_y. \end{aligned} \tag{17}$$

Applying this conversion to eq. (16) gives

$$\begin{aligned} \tilde{A}_x^0(k_x, k_y, z, \omega) = {} & \frac{I\, ds}{2}\left[\frac{1}{u_0}\exp(-u_0|z + h|) + C_0(k_x, k_y, \omega)\exp(u_0 z)\right], \end{aligned} \tag{18}$$

where $C_0 = \hat{C}_0/\sqrt{k_x^2 + k_y^2}$. The boundary conditions in eq.

(15) link the solutions in all the layers, from layer 0 to layer N. Using these boundary conditions, and the general form of $\tilde{A}_x$ in each layer given by eq. (14), a pair of simultaneous equations can be constructed for D_N and C_0. Once D_N and C_0 are known, the coefficients C_j and D_j can be calculated for all layers, hence giving $\tilde{A}_x$ for all z.

The x component of the vector potential, $A_x(x, y, z, \omega)$, is recovered by performing the inverse 2-D Fourier transform. This is evaluated using eq. (17). The y derivative required to give $H_z(x, y, z, \omega)$ from $A_x(x, y, z, \omega)$ (see eq. 5) can be incorporated in this inverse Hankel transform:

$$\begin{aligned} H_z(x, y, z, \omega) &= -\frac{\partial}{\partial y} A_x(x, y, z, \omega) \\ &= -\frac{\partial}{\partial y}\left\{\frac{1}{2\pi}\int_0^\infty \tilde{A}_x(\lambda, z, \omega)\lambda J_0(\lambda r)\, d\lambda\right\} \\ &= -\frac{1}{2\pi}\int_0^\infty \tilde{A}_x(\lambda, z, \omega)\lambda J_0'(\lambda r)\lambda \frac{\partial r}{\partial y}\, d\lambda \\ &= \frac{1}{2\pi}\frac{y}{r}\int_0^\infty \tilde{A}_x(\lambda, z, \omega)\lambda^2 J_1(\lambda r)\, d\lambda, \end{aligned} \tag{19}$$

using eq. (9.1.28) of Abramowitz & Stegun (1970), and λ and r have the same meaning as in eq. (16). Anderson's (1979a) digital filtering code is used to compute the inverse Hankel transform in eq. (19) giving H_z as a function of distance, r, from the electric dipole. This can then be integrated around the rectangular loop in the same way as Poddar (1982) to give the vertical component of the H field induced at any point on the surface of a layered earth by the rectangular transmitter loop. The desired time-domain result of either $h_z(t)$ or $\partial h_z(t)/\partial t$ can be obtained from this frequency dependence of the H field by using the digital filtering technique of Newman, Hohmann & Anderson (1986). Note that it is only in this final transformation that we have to worry about whether we are dealing with the h field or its time derivative: the analysis prior to this transformation is identical for both forms of data in the time domain. The above steps are summarized in the flow diagram in Fig. 2.

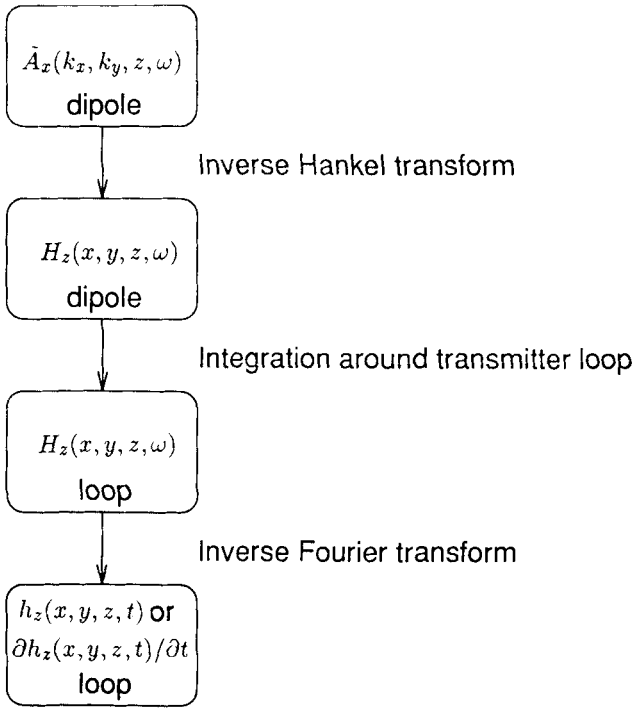

Figure 2. The sequence of integrations used to transform the values of the x component of the vector potential due to a horizontal electric dipole as a function of wavenumber and frequency to values of the vertical component of the h field, or its time derivative, for the rectangular transmitter loop as a function of space and time. This sequence of linear transformations is also used to obtain the sensitivities $\partial h/\partial \sigma_j(x, y, t)$ for the rectangular loop from the values of $\partial \tilde{A}_x/\partial \sigma_j(k_x, k_y, \omega)$ for the dipole.

2.2 Calculation of the sensitivities

To solve the inverse problem, we need to compute the sensitivies that quantify how a change in the conductivity of each layer affects the data. The layered conductivity structure in Fig. 1 can be described in terms of a linear combination,

$$\sigma(z) = \sum_{j=1}^{N} \sigma_j \psi_j(z), \tag{20}$$

where the basis function, ψ_j, is a box car, equal to unity within the jth layer and zero everywhere else. The coefficient, σ_j, is equal to the conductivity of the jth layer. If these coefficients are changed by a small amount, then the resulting value of h_z (or $\partial h_z/\partial t$) measured at the surface of the conductivity structure is given by a Taylor series expansion about the original conductivity structure:

$$h[\sigma + \delta\sigma] = h[\sigma] + \sum_{j=1}^{N} \frac{\partial h[\sigma]}{\partial \sigma_j}\delta\sigma_j + O\,\|\delta\sigma\|^2, \tag{21}$$

where $\sigma = (\sigma_1, \ldots, \sigma_N)^T$ is a vector of coefficients specifying the original conductivity structure, $\delta\sigma = (\delta\sigma_1, \ldots, \delta\sigma_N)^T$ represents the changes in the coefficients, and the first-order partial derivatives are the sensitivities. The square brackets indicate the dependence on the conductivity, and $\|\cdot\|$ represents the l_2 norm. Here, and in most instances throughout the rest of this paper, we take h to represent either h_z or $\partial h_z/\partial t$.

To calculate the sensitivity $\partial h/\partial \sigma_j$, we start by considering the change in $\tilde{A}_x^1(k_x, k_y, z = 0, \omega)$ for the electric dipole source that results from a change in the conductivity of the jth layer. The series of linear transformations (see Fig. 2) used to obtain $h(x, y, z, t)$ from $\tilde{A}_x^j(k_x, k_y, z, \omega)$ can then be used to obtain the desired sensitivity $\partial h/\partial \sigma_j$ for the rectangular loop.

Using the definition of the layered conductivity structure given in eq. (20), and simplifying the notation so that $F(z)$ represents $\tilde{A}_x$, eq. (13) can be rewritten in a form that is valid for all $z \in (-\infty, \infty)$:

$$\left(\frac{d^2}{dz^2} - u_0^2 - i\omega\mu_0 \sum_{j=0}^{N} \sigma_j \psi_j\right) F = S, \tag{22}$$

where $u_0^2 = k_x^2 + k_y^2 - \mu_0\varepsilon_0\omega^2$ and S represents the dipole source in layer 0. Differentiating with respect to σ_j (McGillivray & Oldenburg 1990), making use of the chain rule and realizing that S is independent of σ_j, eq. (22)

becomes

$$\left(\frac{d^2}{dz^2} - u_0^2 - i\omega\mu_0 \sum_{j=0}^{N} \sigma_j \psi_j\right) \frac{\partial F}{\partial \sigma_j} = i\omega\mu_0 \psi_j F, \tag{23}$$

which is just an inhomogeneous ordinary differential equation for the sensitivity, $\partial F/\partial\sigma_j$. The boundary conditions are $\partial F/\partial\sigma_j \to 0$ as $z \to \pm\infty$. This boundary value problem can be solved using the adjoint Green's function method (Lanczos 1961). Hence,

$$\frac{\partial F}{\partial \sigma_j}(\zeta) = \int_{-\infty}^{\infty} i\omega\mu_0 \psi_j(z) F(z) G^{+*}(z;\zeta)\, dz, \tag{24}$$

where the adjoint Green's function $G^+(z;\zeta)$ satisfies

$$\left(\frac{d^2}{dz^2} - u_0^2 + i\omega\mu_0 \sum_{j=0}^{N} \sigma_j \psi_j\right) G^+(z;\zeta) = \delta(z-\zeta) \tag{25}$$

and

$$G^+(z;\zeta) \to 0 \quad \text{as} \quad z \to \pm\infty. \tag{26}$$

To construct the adjoint Green's function, we need two linear independent solutions of the homogeneous form of eq. (25), one of which satisfies the boundary condition as $z \to -\infty$, and the other which satisfies the boundary condition as $z \to +\infty$. For the problem under discussion in this paper, we are only interested in the value of the sensitivity at the surface of the Earth ($\zeta = 0$ in eq. 24). In the region $-\infty < z \le \zeta = 0$, where the conductivity is zero, the adjoint Green's function has the form $\exp(u_0 z)$. In the region $\zeta = 0 \le z < \infty$, eq. (25) is the complex conjugate of eq. (22). And, since $F^* \to 0$ as $z \to +\infty$, the adjoint Green's function is proportional to F^* in this region. Hence,

$$G^+(z;\zeta) = \begin{cases} c^- e^{u_0 z}, & z \le \zeta = 0, \\ c^+ F^*(z), & z \ge \zeta = 0. \end{cases} \tag{27}$$

At $z = \zeta = 0$, $G^+(z;\zeta)$ must be continuous, and its derivative with respect to z must be discontinuous by an amount equal to 1 (Roach 1982). This determines the two coefficients:

$$\begin{aligned} c^- &= \frac{F^*(0)}{F'^*(0) - u_0 F^*(0)}, \\ c^+ &= \frac{1}{F'^*(0) - u_0 F^*(0)}, \end{aligned} \tag{28}$$

where the prime denotes the derivative.

So, using the explicit form of the adjoint Green's function given above, and remembering that ψ_j is unity in the jth layer and zero everywhere else, eq. (24) becomes

$$\left.\frac{\partial F}{\partial \sigma_j}\right|_{\zeta=0} = \frac{i\omega\mu_0}{F'(0) - u_0 F(0)} \int_{z=z_{j-1}}^{z_j} [F(z)]^2\, dz. \tag{29}$$

Then, using eq. (18) to evaluate the denominator, we arrive at the following expression for the sensitivity which links the change in $\tilde{A}_x^1(k_x, k_y, z=0, \omega)$ to the change in the conductivity of the jth layer:

$$\begin{aligned} &\frac{\partial \tilde{A}_x^1}{\partial \sigma_j}(k_x, k_y, \zeta = 0, \omega) \\ &\quad = -\frac{i\omega\mu_0}{I\, ds} \int_{z=z_{j-1}}^{z_j} [\tilde{A}_x^j(k_x, k_y, z, \omega)]^2\, dz. \end{aligned} \tag{30}$$

We can calculate this integral using the results for $\tilde{A}_x^j$ obtained in Section 2.1. And the desired sensitivity, $\partial h/\partial\sigma_j$, can be obtained from $\partial\tilde{A}_x^1/\partial\sigma_j$ by the series of transformations shown in Fig. 2.

3 INVERSION

We consider a set of M observations, $h_i^{(\mathrm{obs})}$, $i = 1, \ldots, M$ which can either be the vertical component of the h field, or its time derivative. These observations could result from measurements at different delay times, or at different locations on the surface of the Earth, or a combination of both. Our goal is to find a set of conductivities that adequately reproduce these observations. Because conductivities found in the Earth can vary over orders of magnitude, it is convenient to work with the logarithm of conductivity in the inverse problem. Also, working with logarithms ensures that σ is positive. We let $m_j = \ln\sigma_j$, and use the vector $\mathbf{m} = (m_1, \ldots, m_N)^{\mathrm{T}}$ to define the model for the inverse problem.

The inverse problem is non-unique: if there is one model that adequately reproduces the finite set of observations, then there is an infinite number of such models. To find a specific model, we minimize an objective function of the model which has the form

$$\phi_m = \|\mathbf{W}_m(\mathbf{m} - \mathbf{m}^{(\mathrm{ref})})\|^2 \tag{31}$$

where $\mathbf{W}_m$ is a weighing matrix and $\mathbf{m}^{(\mathrm{ref})}$ is a reference model. The model, $\mathbf{m}$, that minimizes ϕ_m will have a character that depends on the particular choices for the weighting matrix and the reference model. The reference model can be used to include any *a priori* information that may be available about the possible conductivity structure. We note that the explicit inclusion of a reference model is of particular importance when the model is parameterized in terms of the logarithm of conductivity. If the reference model were omitted from ϕ_m, the implicit reference conductivity of $1\ \mathrm{S\,m^{-1}}$ could severely bias the inversion results.

The numerical values for $\mathbf{W}_m$ can be generated by deciding what type of model is to be found. This is easily accomplished by considering a functional analogous to ϕ_m for models that are continuous functions of depth, for example,

$$\Phi_m = \int_{z=0}^{\infty} w(z)\, |T[m(z) - m^{(\mathrm{ref})}(z)]|^2\, dz. \tag{32}$$

The operator T can be the identity operator, or the first or second order derivative with respect to z. The function $w(z)$ is an additional weighting function which can be used to enhance or suppress structure over certain depth ranges. The weighting matrix $\mathbf{W}_m$ can be obtained by making ϕ_m the discrete equivalent of Φ_m.

To determine whether or not the data produced by our model conductivity structure are sufficiently close to the observations, we introduce the following measure of misfit:

$$\phi_d = \|\mathbf{W}_d[\mathbf{h}^{(\mathrm{obs})} - \mathbf{h}^{(\mathrm{pred})}]\|^2, \tag{33}$$

where $\mathbf{h}^{(\mathrm{pred})}$ is the vector made up of the data predicted from the model, and $\mathbf{W}_d^{\mathrm{T}}\mathbf{W}_d = \mathbf{C}_d^{-1}$, where $\mathbf{C}_d$ is the covariance matrix. Our objective in the inversion is to find a model which gives a misfit, ϕ_d, equal to a target misfit $\phi_d^{(\mathrm{tar})}$.

For the examples used here, we will assume that the data errors are unbiased, independent and Gaussian. In such cases, $\mathbf{W}_d$ is a diagonal matrix whose elements are the reciprocals of the standard deviation of each datum, and ϕ_d is equal to the χ^2 random variable. From the properties of the χ^2 random variable, the expected value of ϕ_d is equal to M, the number of observations. Hence, our final target misfit in the inverse problem is $\phi_d^{(\mathrm{tar})} = M$.

The relationship between the observations and the model conductivity structure is non-linear and so an iterative method is required to solve the inverse problem. At the $(n+1)^{\mathrm{th}}$ iteration,

$$\phi_d^{(n+1)} = \|\mathbf{W}_d(\mathbf{h}^{(\mathrm{obs})} - \mathbf{h}^{(n+1)})\|^2. \tag{34}$$

Using the Taylor series expansion in eq. (21), this can be approximated by

$$\phi_d^{\mathrm{L}} = \|\mathbf{W}_d[\mathbf{h}^{(\mathrm{obs})} - \mathbf{h}^{(n)} - \mathbf{D}\delta\mathbf{m}]\|^2, \tag{35}$$

where $D_{ij} = \partial h_i/\partial m_j = \sigma_j\, \partial h_i/\partial \sigma_j$, since the model is now defined in terms of the natural logarithm of conductivity. The superscript L distinguishes this linearized estimate of the misfit from the true misfit defined in eq. (34). We shall make use of ϕ_d^{L} in the solution of the linear system of equations at each iteration, but it is $\phi_d^{(n)}$ that is the true measure of how the iterative scheme is progressing. By writing $\delta\mathbf{m}$ explicitly as the difference between the model parameters at two successive iterations (e.g. Oldenburg, 1983; Constable, Parker & Constable 1987), and introducing the reference model, eq. (35) becomes

$$\begin{aligned}\phi_d^{\mathrm{L}} &= \|\mathbf{W}_d[\mathbf{h}^{(\mathrm{obs})} - \mathbf{h}^{(n)} - \mathbf{D}\mathbf{m}^{(\mathrm{ref})} + \mathbf{D}\mathbf{m}^{(\mathrm{ref})} - \mathbf{D}\mathbf{m}^{(n+1)} + \mathbf{D}\mathbf{m}^{(n)}]\|^2 \\ &= \|\mathbf{d}^{(n)} - \hat{\mathbf{D}}\hat{\mathbf{m}}^{(n+1)}\|^2,\end{aligned} \tag{36}$$

where

$$\begin{aligned}\mathbf{d}^{(n)} &= \mathbf{W}_d[\mathbf{h}^{(\mathrm{obs})} - \mathbf{h}^{(n)} - \mathbf{D}\mathbf{m}^{(\mathrm{ref})} + \mathbf{D}\mathbf{m}^{(n)}], \\ \hat{\mathbf{D}} &= \mathbf{W}_d\mathbf{D}\mathbf{W}_m^{-1}, \\ \hat{\mathbf{m}}^{(n+1)} &= \mathbf{W}_m[\mathbf{m}^{(n+1)} - \mathbf{m}^{(\mathrm{ref})}].\end{aligned} \tag{37}$$

Hence, the linearized inverse problem to be solved at the $(n+1)^{\mathrm{th}}$ iteration is:

minimize

$$\phi_m = \|\hat{\mathbf{m}}^{(n+1)}\|^2 \tag{38}$$

subject to the constraint that

$$\phi_d^{\mathrm{L}} = \|\mathbf{d}^{(n)} - \hat{\mathbf{D}}\hat{\mathbf{m}}^{(n+1)}\|^2 = \phi_d^{(\mathrm{tar})}. \tag{39}$$

This problem could be solved by differentiating the objective function

$$\phi = \phi_m + \alpha[\phi_d^{\mathrm{L}} - \phi_d^{(\mathrm{tar})}] \tag{40}$$

with respect to the elements of $\mathbf{m}^{(n+1)}$ and equating to zero (α is a Lagrange multiplier). This would create an $N \times N$ system of equations to be solved for $\mathbf{m}^{(n+1)}$. However, in this paper, we use the more computationally efficient method of singular value decomposition (SVD) and exploit the fact that the SVD solution of an underdetermined system of equations is the one with the smallest l_2 norm (Wiggins 1972; Parker 1977; Menke 1984; Golub & Van Loan 1989).

The SVD of the matrix $\hat{\mathbf{D}}$ is $\hat{\mathbf{D}} = \mathbf{U}\Lambda\mathbf{V}^T$. The solution to the linearized inverse problem in eqs (38) and (39) is then given by

$$\hat{\mathbf{m}}^{(n+1)} = \mathbf{V}\mathbf{T}\Lambda^{-1}\mathbf{U}^T\mathbf{d}^{(n)} \tag{41}$$

where $T_{ij} = \alpha s_i^2\delta_{ij}/(\alpha s_i^2 + 1)$, s_i is the ith singular value of $\hat{\mathbf{D}}$ and δ_{ij} is the Kronecker delta (Wiggins 1972). The Lagrange multiplier α (the same as that in eq. (40) above) could be chosen using a line search so that the constraint $\phi_d^{\mathrm{L}} = \phi_d^{(\mathrm{tar})}$ in eq. (39) is satisfied. However, it is a solution to the full non-linear inverse problem that we require. We, therefore, use the line search and forward modelling to choose α such that $\phi_d^{(n+1)} = \phi_d^{(\mathrm{tar})}$. Finally, since the linearized inverse problem defined by eqs (38) and (39) is only an approximation to the full non-linear problem, it is prudent to set the target misfit at each iteration to be some fraction β of the misfit resulting from the previous iteration. So, at the $(n+1)^{\mathrm{th}}$ iteration, $\phi_d^{(\mathrm{tar})}$ is chosen to be $\max[\beta\phi_d^{(n)}, M]$ where β is typically $0.1 \leq \beta \leq 0.5$.

We shall now apply the above iterative procedure to both synthetic and field data.

4 EXAMPLES

4.1 Synthetic data

Synthetic data were generated from the three-layered conductivity structure shown in Fig. 3. The transmitter loop was a square of side 50 m and the vertical component of the h field due to a step turn-off in a 1 A current was calculated 50 m from the centre of the loop. Only a pure step turn-off in the transmitter current was considered: no linear ramp was included. Both the transmitter and the receiver lay on the surface of the conductivity structure, and 20 values of h_z were calculated over the range of delay times shown in Fig. 4. Gaussian random noise with a standard deviation of 2.5 per cent was added to the values of h_z. The data, with estimated error bars, are shown in Fig. 4.

The inversion routine was used to obtain three different conductivity models, each with a distinct character, that reproduced the synthetic data to a similar level of misfit. These three models minimize, in turn, the difference between the model and a reference half-space of $5 \times 10^{-2}\,\mathrm{S\,m^{-1}}$, the gradient of the model, and the curvature. For convenience, we refer to them generically as the smallest, flattest, and smoothest models. The controlling factor for each model is the weighting matrix, $\mathbf{W}_m$. For the smallest model,

$$\mathbf{W}_m = \mathrm{diag}\,(\sqrt{l_1}, \sqrt{l_2}, \ldots, \sqrt{l_{N-1}}, \sqrt{l_{N-1}}), \tag{42}$$

where l_j is the thickness of the jth layer. The final element of $\mathbf{W}_m$, which corresponds to the basement half-space, is given the same value as the previous element.

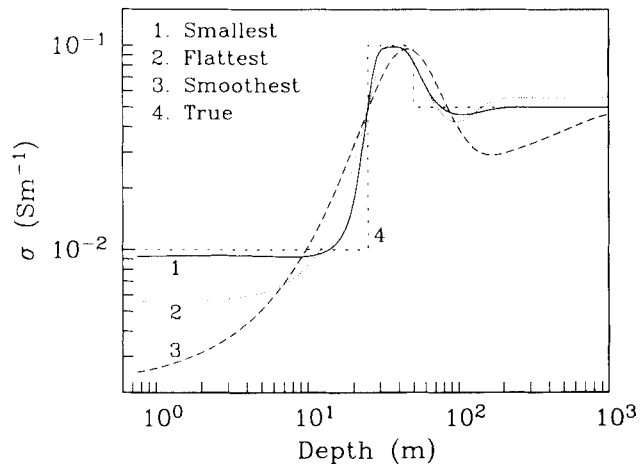

Figure 3. The three-layer model ('true') used to generate the synthetic data, and the three models produced by the inversion routine. For clarity, the individual layers in the smallest, flattest and smoothest models are not shown.

The weighting matrix for the flattest model is

$$\mathbf{W}_m = \begin{bmatrix} \left(\frac{l_1+l_2}{2}\right)^{-1/2} & -\left(\frac{l_1+l_2}{2}\right)^{1/2} & 0 & \cdots & 0 \\ 0 & \left(\frac{l_2+l_3}{2}\right)^{1/2} & -\left(\frac{l_2+l_3}{2}\right)^{1/2} & 0 & \\ \vdots & & & & \vdots \\ & & 0 & (l_{N-1})^{1/2} & -(l_{N-1})^{-1/2} \\ 0 & \cdots & & 0 & C \end{bmatrix} \quad (43)$$

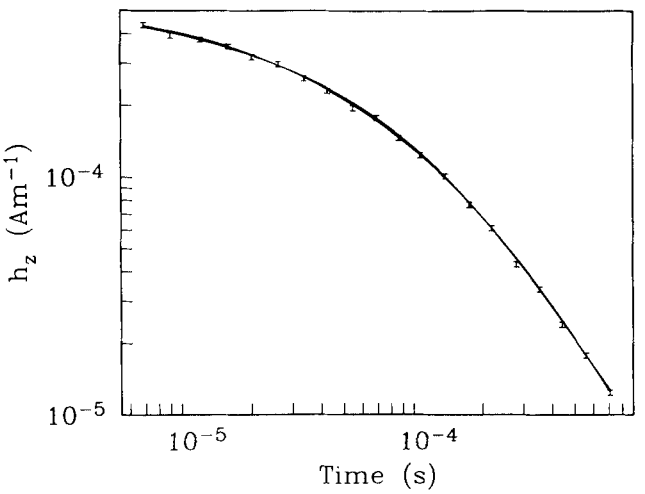

Figure 4. The synthetic data, and associated error bars, generated from the three-layer model in Fig. 3. The values of h_z were calculated 50 m from the centre of a 50 m × 50 m transmitter loop. A pure step turn-off in a 1 A current was used as the transmitter current waveform and Gaussian random noise of standard deviation 2.5 per cent was incorporated into the data. The continuous curves represent the data predicted by each of the three models shown in Fig. 3 that resulted from the inversion.

where the constant, C, was chosen as $10^{-3}(l_{N-1})^{-1/2}$. This value is effectively negligible compared with the other elements in the matrix, and yet is sufficiently large so that $\mathbf{W}_m^{-1}$ can be computed. For the smoothest model, the weighting matrix is the square of the matrix used for the flattest model.

The resulting three models are shown in Fig. 3. All have 100 layers ($N = 100$), with the thicknesses increasing exponentially (to the base 1.05 with the thickness of the first layer equal to 0.5 m). During the inversion process, β (the desired reduction in misfit at each iteration) was kept fixed at 0.5. This gave a slow but steady convergence towards the final model.

The forward calculations from the three models produced by the inversion routine are represented by the continuous lines in Fig. 4. The values of ϕ_d for the smallest, flattest and smoothest models were 20.0, 20.1 and 20.3 respectively ($M = 20$). Although these three values represent an equivalent fit to the data, the models are noticeably different in character. These different characters are a direct consequence of the particular model norm that was minimized in the inversion. The most obvious differences appear in the depth ranges that are poorly constrained by the data: below approximately 200 m the smallest model returns to its reference half-space of 5×10^{-2} S m^{-1}, the flattest model levels out to achieve zero gradient, and the smoothest model degenerates to a straight line when no longer influenced by the data. Similar behaviours can be seen at shallow depths above about 10 m. Even in the depth range to which the data are most sensitive (10–200 m, approximately) there are differences in character between the three models. The smallest model manages to follow the block nature of the true model quite closely, whereas the smoothest model smears out the high conductivity layer as much as it can in order to produce the model with the minimum amount of curvature.

From Fig. 3 it is obvious that the smallest model is the closest to the 'true' Earth. However, the remarkable agreement above 10 m depth is somewhat fortuitous, since the model at these depths is very poorly constrained by the data, and the behaviour of the model is dominated by ϕ_m. And the exact agreement below 200 m is only to be expected since we chose our reference model to have the same conductivity as the basement half-space in the true Earth. In general, we found that the smallest model often contained too much unrealistic structure, and that a minimum structure model gave the most plausible representation of the true Earth. In particular, the tendency of the flattest model to cause less smearing out of abrupt changes in conductivity compared with the smoothest model, as shown in Fig. 3, and the obvious levelling off when no longer constrained by the data, made the flattest model our preferred choice in many cases.

4.2 Field data

To test the inversion routine with more realistic data, we inverted two sets of field data acquired during an environmental study. Values of the time derivative of the vertical component of the h field were measured at the centre of a square (60 m × 60 m) transmitter loop using the Geonics Protem system. The data, and their assumed errors,

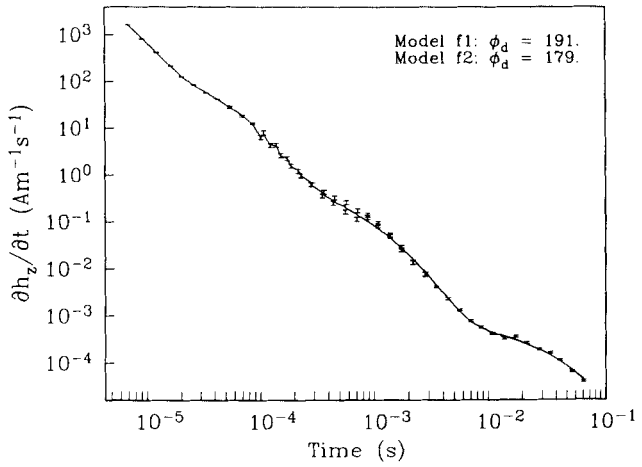

Figure 5. A TEM sounding acquired during an environmental survey. The transmitter loop was 60 m × 60 m, and the receiver was at its centre. The data were acquired in three overlapping sweeps: 7 μs–0.7 ms, 0.1–2.8 ms, and 0.8–70 ms. The observations and assigned measurement errors are represented by the error bars. The continuous curve indicates the data predicted from both models f1 and f2 in Fig. 7.

obtained from soundings at two different locations are presented in Figs 5 and 6.

The Protem instrument uses a linear ramp turn-off of length τ instead of the pure step turn-off, which is impossible to generate in practice. This modification of the source current waveform can be taken into account when calculating the resultant time decay of the fields by convolving a boxcar of length τ and height $1/\tau$ with the values of $\partial h_z/\partial t$ calculated for a pure step-off current source (Asten 1987). The observations shown in both Figs 5 and 6 were acquired in three overlapping sweeps, the first sweep from 7 μs to 0.7 ms, the second from 0.1 to 2.8 ms, and the third from 0.8 ms onwards. The length of the ramp, τ, for these sweeps was 3.5 μs, 35 μs and 45 μs, respectively.

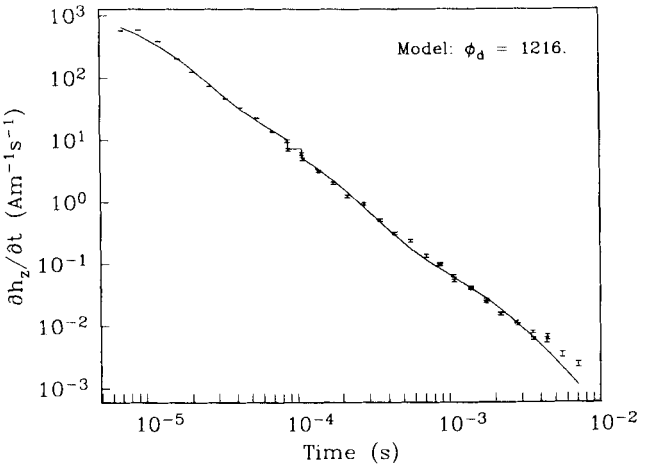

Figure 6. A second sounding from an environmental survey. The survey geometry and the three measurement sweeps are the same as for Fig. 5. The error bars indicate the observations and assigned measurement errors, and the continuous curve represents the predicted data from the flattest model produced by the inversion, and shown in Fig. 8.

These different ramp times give the data a somewhat sawtooth appearance in the time range for which the sweeps overlap.

The linear ramp turn-off in the transmitter current must also be taken into account in the inversion process. Because we are carrying out the inversion in the time domain, the sensitivities required for a ramp turn-off in the transmitter current can be obtained by applying the above convolution to the sensitivities calculated for the pure step turn-off.

For the data in Fig. 5, errors of 1 per cent, 10 per cent and 5 per cent were assigned to early, mid and late time measurements, respectively. For the data in Fig. 6, errors of 1 per cent were assigned to early time measurements, errors of 5 per cent to intermediate time measurements and errors of 10 per cent to the last few measurements.

Fig. 7 shows two inversion results for the data in Fig. 5. Model f1, represented by solid line, was obtained using the same weighting matrix as for the flattest model in Section 4.1. Model f2, represented by the dotted line, was obtained using the weighting matrix

$$\mathbf{W}_m = \begin{pmatrix} 1 & -1 & 0 & \cdots & 0 \\ 0 & 1 & -1 & & \vdots \\ & & \ddots & & \\ \vdots & & & 1 & -1 \\ 0 & \cdots & & 0 & C \end{pmatrix} \tag{44}$$

where $C = 10^{-3}$. Both models have 200 layers increasing exponentially in thickness (to the base 1.03, with the first layer of thickness 0.1 m). Because of this increasing layer thickness, the model norm constructed using $\mathbf{W}_m$ above is essentially a discretized version of

$$\Phi_m = \int_{z=0}^{\infty} \left[\frac{d(\ln \sigma)}{d(\ln z)}\right]^2 d(\ln z) = \int_{z=0}^{\infty} z\left[\frac{d(\ln \sigma)}{dz}\right]^2 dz. \tag{45}$$

Similarly, the model norm constructed using $\mathbf{W}_m$ in eq. (43) is a discretized version of

$$\Phi_m = \int_{z=0}^{\infty} \left[\frac{d(\ln \sigma)}{dz}\right]^2 dz. \tag{46}$$

The dashed line in Fig. 7 corresponds to the result obtained from a parameter estimation program (TEMEX-GL) based on (Anderson 1979b) which was restricted to contain seven layers.

The values of the misfit ϕ_d for models f1 and f2 were 191 and 179, respectively. The value of ϕ_d for the seven-layer model was 983. Models f1 and f2 produce nearly identical fits to the observations, as illustrated in Fig. 5. However, the two values of misfit quoted above are still significantly larger than the expected value of 56 (the number of observations). No model could be found which gave a smaller misfit than that for model f2. This suggests that the errors we assigned to the data are smaller than the true uncertainties in the measurements. This seems entirely plausible, especially for the late time measurements, where uncertainties of 30 or 40 per cent are more likely to be realistic.

The similarity between the two models in Fig. 7, despite the different nature of the weighting matrices used to produce them, emphasizes the robustness of an inversion routine which looks for a minimum structure model. Since

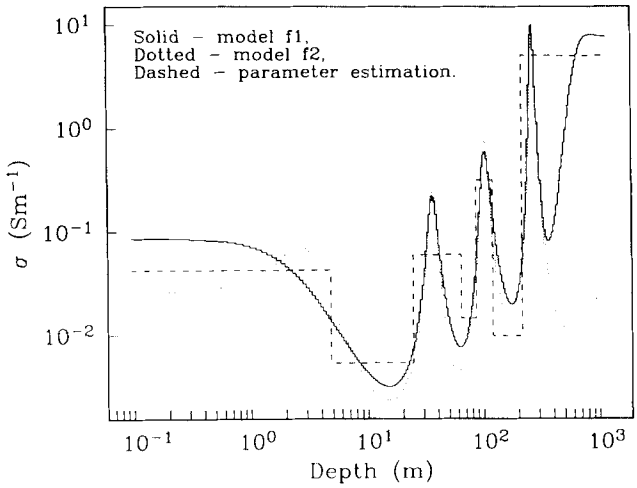

Figure 7. f1 and f2 are the two versions of the flattest model obtained from the inversion of the data in Fig. 5. The best-fitting seven-layer model produced by a parameter estimation routine (TEMEX-GL) is also shown.

models f1 and f2 both contain just enough structure to fit the data, it is not surprising that they agree on the features that are required by the data. This provides confidence that the particular sequence of conductive and resistive layers to a depth of about 300 m is present in the real Earth.

Below 300 m the models are poorly constrained by the observations, and so the particular form of the weighting matrix dominates their behaviour. The weighting term, z, that appears in eq. (45) but not (46), therefore, causes structure in model f2 to be suppressed at these depths compared with model f1. However, the fact that both models f1 and f2 do show increases in conductivity around 500 m depth, rather than levelling off, might indicate the presence of a good conductor on the extreme limit of penetration of this sounding. At shallow depths, the different weighting matrices lead to structure being enhanced in model f2 relative to model f1.

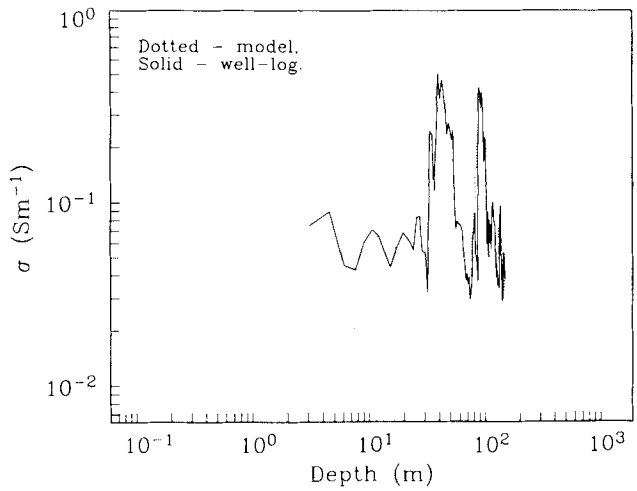

Figure 8. The flattest model (dotted line) obtained from the inversion of the data in Fig. 6. The solid line represents the values of the conductivity measured in a borehole 70 m from the observation site.

As a final example, the data from the second sounding (see Fig. 6) were inverted. The weighting matrix was the same as the one used to produce model f2 in Fig. 7. The resulting model is represented by the dotted line in Fig. 8. It is again made up of 200 layers whose thicknesses increase exponentially with depth. The solid line in Fig. 6 represents the data predicted by this model. The corresponding value of the misfit was $\phi_d = 1216$. The assigned uncertainties again seem to be too small and it was impossible to obtain a misfit close to the expected value of 40. The solid line in Fig. 8 represents well-log measurements of conductivity obtained from a borehole 70 m away from the location of the sounding. There is very good agreement between the model and the well-log measurements in the depth range 10–150 m, especially on the location of the upper regions of the two conductive zones around 35 and 90 m. The character of the well-log, comprising transition zones rather than a few layers of constant conductivity, is also reproduced by the model in Fig. 8. This type of model, constructed by minimizing the l_2 norm of its gradient, therefore, seems particularly suited to this geological setting.

5 DISCUSSION

In this paper, we have presented an inversion algorithm that generates a layered conductivity structure from measurements of h_z or $\partial h_z/\partial t$ as functions of time. Our inversion operates on data in the time-domain, despite the fact that a large part of the computations take place in the frequency domain. Our approach requires many more transformations between the frequency- and time domains than the alternative strategy of transforming the data to the frequency domain before inversion. However, the time required for these transformations is only a fraction of that required to generate the sensitivities as functions of frequency. Moreover, working with data in the time domain avoids the question of how to transform a limited number of data points and associated measurement errors to the frequency domain without loss of information. The extra effort required to carry out the inversion in the time-domain, therefore, allows full use to be made of the measurement errors, both in deciding how well the data should be fit, and in determining the relative importance of each datum in the inversion. One further advantage of the approach presented in this paper is the ease with which an arbitrary transmitter current waveform can be incorporated by convolution in the time domain: we simply convolve the waveform with both the predicted data and sensitivities calculated from an impulsive current source.

We used singular value decomposition (SVD) to solve the linear system of equations at each iteration: from the properties of SVD, such a solution to an underdetermined system of equations is the minimum l_2 norm solution. This technique is more computationally efficient than inverting the $N \times N$ system of equations obtained by explicitly minimizing an objective function with respect to the model parameters.

The formulation we have presented is quite general in its ability to generate different conductivity models. The choice of weighting matrix, reference model and norm provides a great deal of flexibility in tailoring the constructed model so that it is consistent with any prior geological and geophysical

information. In this paper, we have only considered a weighted l_2 norm. This results in conductivity structures that change somewhat slowly with depth. Other norms are possible. For example, the l_1 norm used by Dosso & Oldenburg (1989) to minimize the total variation of the conductivity as a function of depth in the inversion of magnetotelluric data produces models that are blocky in character. This is preferable if the local geology is known to be made up of distinct, contrasting layers. This is an assumption that is often made when inverting data. However, the character of the well-log in Fig. 8 is more in keeping with transition zones rather than abrupt jumps between neighbouring layers and the minimum structure model obtained using the l_2 norm mimics these gradual changes very well.

As a final comment, we mention that we have worked completely with the physical quantities that are measured in a TEM survey, either h_z or $\partial h_z/\partial t$, rather than working with an apparent conductivity. This means that the inversion routine presented here can be applied to the response for any source–receiver geometry, for which, typically, the transformation to apparent conductivity is multivalued, and, hence, not easy to carry out.

ACKNOWLEDGMENTS

We are extremely grateful to Cliff Candy of Frontier Geosciences, Inc., for supplying the field data, the well-log measurements and the results of the TEMEX-GL program (Interprex, Ltd.). C.G.F. would like to acknowledge receipt of a Commonwealth Scholarship. This research was supported by NSERC grant 5-84270.

REFERENCES

Abramowitz, M. & Stegun, I. A., 1970. *Handbook of Mathematical Functions*, Dover Publications, New York.

Anderson, W. L., 1979a. Numerical integration of related Hankel transforms of orders 0 and 1 by adaptive digital filtering, *Geophysics*, **44,** 1287–1305.

Anderson, W. L., 1979b. Programs TRANS_HCLOOP and TRANS_HZWIRE: calculation of the transient horizontal coplanar loop soundings and transient wire-loop soundings, *USGS Open-File Report 79–590.*

Anderson, W. L., 1982. Adaptive non-linear least-squares solution for constrained or unconstrained minimization problems (Subprogram NLSOL), *USGS Open-File Report 82–68.*

Anderson, W. L., 1985. Computation of transient soundings for the time-derivative of H_z near a rectangular loop source on a layered earth (Program FWDTHZ), *USGS Open-File Report 85–270.*

Asten, M. W., 1987. Full transmitter waveform transient electromagnetic modeling and inversion for soundings over coal measures, *Geophysics*, **52,** 279–288.

Constable, S. C., Parker, R. L. & Constable, C. G., 1987. Occam's inversion: a practical algorithm for generating smooth models from electromagnetic sounding data, *Geophysics*, **52,** 289–300.

Dosso, S. E. & Oldenburg, D. W., 1989. Linear and non-linear appraisal using extremal models of bounded variation, *Geophys. J. Int.*, **99,** 483–495.

Eaton, P. A. & Hohmann, G. W., 1989. A rapid inversion technique for transient electromagnetic soundings, *Phys. Earth. planet. Inter.*, **53,** 384–404.

Fullagar, P. K., 1983. Backus–Gilbert inversion of SIROTEM soundings, *Abstracts: The Third Biennial Conference of the ASEG*, pp. 28–30.

Fullagar, P. K., 1989. Generation of conductivity–depth pseudosections from coincident loop and in-loop TEM data, *Expl. Geophys.*, **20,** 43–45.

Fullagar, P. K. & Oldenburg, D. W., 1984. Inversion of horizontal loop electromagnetic frequency soundings, *Geophysics*, **49,** 150–164.

Golub, G. H. & Van Loan, C. F., 1989. *Matrix Computations*, The John Hopkins University Press, Baltimore.

Huang, H. & Palacky, G. J., 1991. Damped least-squares inversion of time-domain airborne EM data based on singular value decomposition, *Geophys. Prosp.*, **39,** 827–844.

Kaufman, A. A. & Keller, G. V., 1983. *Frequency and Transient Soundings*, Elsevier, Amsterdam.

Lanczos, C., 1961. *Linear Differential Operators*, Van Nostrand, London.

McGillivray, P. R. & Oldenburg, D. W., 1990. Methods for calculating Fréchet derivatives and sensitivities for the non-linear inverse problem: a comparative study, *Geophys. Prosp.*, **38,** 499–524.

Macnae, J. & Lamontagne, Y., 1987. Imaging quasi-layered conductive structures by simple processing of transient electromagnetic data, *Geophysics*, **52,** 545–554.

Menke, W., 1984, *Geophysical Data Analysis: Discrete Inverse Theory*, Academic Press, Orlando.

Nabighian, M. N. & Macnae, J. C., 1991. Time-domain electromagnetic prospecting methods, in *Electromagnetic Methods in Applied Geophysics*, Vol. 2, pp. 427–479, ed. Nabighian, M. N., Soc. Expl. Geophys., Tulsa.

Nekut, A. G., 1987. Direct inversion of time-domain electromagnetic data, *Geophysics*, **52,** 1431–1435.

Newman, G. A., Hohmann, G. W. & Anderson, W. L., 1986. Transient electromagnetic response of a three-dimensional body in a layered Earth, *Geophysics*, **51,** 1608–1627.

Oldenburg, D. W., 1983. Funnel functions in linear and non-linear appraisal, *J. geophys. Res.*, **88,** 7387–7398.

Parker, R. L., 1977. Understanding inverse theory, *Ann. Rev. Earth planet. Sci.*, **5,** 35–64.

Poddar, M., 1982. A rectangular loop source of current on a two-layered Earth, *Geophys. Prosp.*, **30,** 101–114.

Raiche, A. P., Jupp, D. L. B., Rutter, H. & Vozoff, K., 1985. The joint use of coincident loop transient electromagnetic and Schlumberger sounding to resolve layered structures, *Geophysics*, **50,** 1618–1627.

Roach, G. F., 1982. *Green's Functions*, Cambridge University Press, Cambridge.

Ward, S. H. & Hohmann, G. W., 1988. Electromagnetic theory for geophysical applications, in *Electromagnetic Methods in Applied Geophysics*, Vol. 1, pp. 131–311, ed. Nabighian, M. N., Soc. Expl. Geophys., Tulsa.

Wiggins, R. A., 1972. The general linear inverse problem: Implication of surface waves and free oscillations for Earth structure, *Rev. Geophys. Space Phys.*, **10,** 251–285.